Appl. Phys. B, 1-8(2006) DOI: 10.1007/s00340-006-2230-1
The original publication is available at www.springerlink.com.

Chromatic aberration in petawatt-class lasers

Hans-Martin Heuck[1,2], **Paul Neumayer**[2,3], **Thomas Kühl**[2,4], **Ulrich Wittrock**[1]

[1] Mnster University of Applied Sciences, Stegerwaldstr. 39, 48565 Steinfurt, Germany
(Fax: +49-2551/962-705, E-Mail: heuck@fh-muenster.de, telephone number: +49-2551/962-332)
[2] Gesellschaft für Schwerionenforschung, Planckstr. 1, 64291 Darmstadt, Germany
(Fax: +49-6159/71-3714, E-Mail: p.neumayer@gsi.de, telephone number: +49-6159-2560)
[3] Julius Maximilian Universität Würzburg, Physikalisches Institut, Am Hubland, 97074 Würzburg, Germany
[4] Universität Mainz, Institut fr Physik, 55099 Mainz

Received: 15 December

Abstract In order to avoid optical damage and non-linear effects, high-power high-energy lasers of the petawatt class like PHELIX (Petawatt High Energy Laser for Heavy-Ion Experiments) use large aperture optics. Usually chromatic aberration associated with these optical elements is neglected. By means of numerical simulations we show how the chromatic aberration affects the focal intensity pattern. In particular, we make quantitative predictions on how chromatic aberration decreases the focused peak intensity. Furthermore, we prove the feasibility of a new interferometer that measures the temporal pulse front distortions which arise from expansion telescopes. We also propose a scheme that pre-compensates these distortions.

PACS:42.65.Re, 42.60.Jf

1 Introduction

In the last decade, ultra-high peak intensity laser systems have opened the path to exciting new experimental possibilities like the acceleration of high-energy particle beams, x-ray generation, or the exploration of relativistic plasma physics [1–4]. The realization of pulse peak powers in excess of $1\,\mathrm{PW} = 10^{15}$ Watt has been enabled by the invention of chirped pulse amplification (CPA) [5,6]. Based on this scheme, several petawatt-class laser systems have been built or are currently under construction [7]. The CPA technique consists in temporally stretching a short pulse from an oscillator by a factor of 10^4 before amplifying it to the desired pulse energy. This way the peak intensity in the laser system during amplification is lowered, thus avoiding damage and pulse distortion due to non-linear effects. Finally, the energetic pulse is compressed to a pulse duration close to the original value.
A typical ultra-high peak power laser system includes a number of Keplerian telescopes to provide spatial filtering, relay imaging of the non-Gaussian intensity distribution and magnification of the beam. These telescopes require positive lenses of up to 0.5 meters in diameter. Unless achromatic lenses are employed, this leads to a gradually increasing amount of chromatic aberration. It was first pointed out by Bor [8] that chromatic aberration leads to a curved pulse front in the near-field which causes an increase of the pulse duration in the focus. Thus chromatic aberration can drastically affect the performance of ultra-high intensity laser systems by reducing the focal intensity achievable in absence of chromatic aberrations[9,10]. To quantitatively predict the impact, a full wave-optics solution of the short-pulse propagation is required. Numerical solutions of the spatio-temporal intensity distribution in the focus of a singlet lens in the presence of chromatic aberration have been shown by Kempe et al. [11,12], while Fuchs et al. analyzed the temporal focusing properties of different lenses for imaging systems [13].
In this paper, we present a more detailed study on the impact of chromatic aberration on the intensity distribution in the focal area including additional effects like spatial phase aberrations and non-Gaussian intensity shapes for typical beam parameters found in ultra-high peak power lasers. For this purpose, we have developed a numerical model that calculates the wave propagation of a coherent, broad-band laser pulse, similar to the one employed in [13]. We propose to pre-compensate the chromatic aberration in ultra-high peak power laser chains at a small beam diameter and offer two simple and yet powerful pre-compensation set-ups. Finally, we demonstrate the use of a self-referencing shifted-field autocorrelator to measure the pulse front distortion that due to chromatic aberration.

2 Chromatic aberration in a high peak power laser

2.1 Chromatic aberration and pulse time delay

We define the chromatic aberration of a broad-band laser beam by a wavelength-dependent wavefront radius-of-curvature $R(\lambda)$, where the curvature $\xi(\lambda) = 1/R(\lambda)$ varies in first-order approximation linearly with the wavelength λ around the center

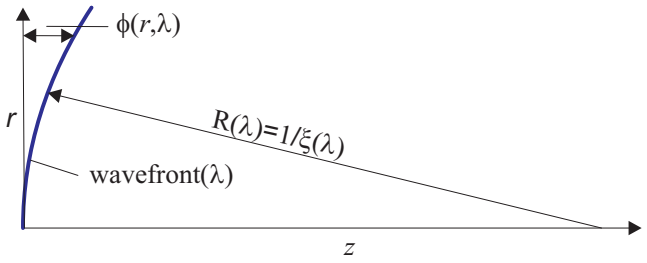

Fig. 1: Phase $\phi(r,\lambda)$ and radius of curvature $R(\lambda)$ of a wavefront with wavelength λ

wavelength λ_0:

$$\xi(\lambda) = \xi_0 + \left.\frac{\mathrm{d}\xi}{\mathrm{d}\lambda}\right|_{\lambda_0} \cdot (\lambda - \lambda_0). \tag{1}$$

Here ξ_0 is the wavefront curvature at λ_0. Focusing a beam with chromatic aberration as defined in Eq. (1) with a lens of focal length $f(\lambda)$ leads to a wavelength-dependent shift of the focal position:

$$\Delta z(\lambda) \approx f_0^2 \left.\frac{\mathrm{d}\xi}{\mathrm{d}\lambda}\right|_{\lambda_0} \cdot (\lambda - \lambda_0). \tag{2}$$

The phase of the curved wavefront at the radial distance $r \ll R(\lambda)$ from the optical axis is given by, see Fig. 1:

$$\phi(r,\lambda) \approx \frac{\pi\xi(\lambda)}{\lambda} \cdot r^2. \tag{3}$$

In vacuum, this results in a radially varying group delay of

$$\begin{aligned} T(r) &= \frac{\mathrm{d}\phi}{\mathrm{d}\omega} = \frac{-\lambda^2}{2\pi c} \cdot \left.\frac{\mathrm{d}\phi}{\mathrm{d}\lambda}\right|_{\lambda_0} \\ &= \frac{r^2}{2c}\left(\xi_0 - \lambda_0 \left.\frac{\mathrm{d}\xi}{\mathrm{d}\lambda}\right|_{\lambda_0}\right), \end{aligned} \tag{4}$$

which causes a distortion of the pulse front. Here c is the vacuum speed of light. Equation (4) yields a paraboloidal pulse front with the curvature being the sum of the wavefront curvature ξ_0 of the center wavelength and an additional curvature as a consequence of chromatic aberration $\left.\frac{\mathrm{d}\xi}{\mathrm{d}\lambda}\right|_{\lambda_0}$ (see Fig. 2):

$$T_{\mathrm{CA}}(r) = -\frac{r^2}{2c} \cdot \lambda_0 \left.\frac{\mathrm{d}\xi}{\mathrm{d}\lambda}\right|_{\lambda_0}. \tag{5}$$

We define the pulse time delay T_{PTD} as the delay of the beam edge at radius $r_{\max}$ with respect to the central part of the beam:

$$T_{\mathrm{PTD}} := T_{\mathrm{CA}}(r_{\max}) - T_{\mathrm{CA}}(0). \tag{6}$$

We will show in the next sections that this quantity adequately describes the impact of chromatic aberration in a high-power laser system. Therefore, we will use this quantity throughout the rest of this paper as an alternative definition for chromatic aberration.
As a specific example, the chromatic aberration of a singlet

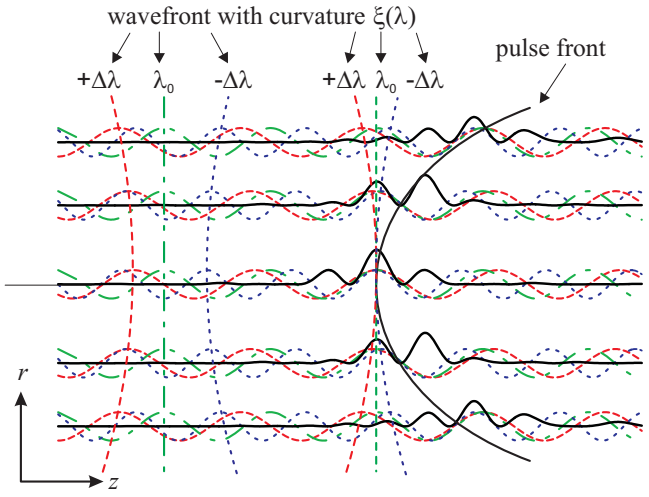

Fig. 2: Wavelength dependent wavefront curvatures result in a radially varying delay $T(r)$ of the pulse front, Eq. (4). Here $\xi_0 = 0$.

lens of focal length $f(\lambda) \approx f_0 + \left.\frac{\mathrm{df}}{\mathrm{d}\lambda}\right|_{\lambda_0} \cdot (\lambda - \lambda_0)$ will turn plane waves into spherical waves with a wavelength-dependent radius of curvature $1/\xi(\lambda) = R(\lambda) = f(\lambda)$. With

$$\frac{\mathrm{d}f}{\mathrm{d}\lambda} = -\frac{1}{\xi^2(\lambda)} \cdot \frac{\mathrm{d}\xi}{\mathrm{d}\lambda} \quad \text{and} \quad \frac{\mathrm{d}f}{\mathrm{d}\lambda} = \frac{-f_0}{(n_0 - 1)} \frac{\mathrm{d}n}{\mathrm{d}\lambda},$$

the pulse time delay of a singlet lens is

$$T_{\mathrm{PTD,lens}} = \frac{-\lambda_0}{2cf_0(n_0 - 1)} \left.\frac{\mathrm{d}n}{\mathrm{d}\lambda}\right|_{\lambda_0} \cdot r_{\max}^2, \tag{7}$$

where n_0 is the refractive index of the lens material at λ_0. This equation has first been derived by Bor [8] and was discussed in the context of short-pulse lasers in the ultra-violet ($\lambda_0 = 249$ nm, BK7: $\lambda_0 \left.\frac{\mathrm{d}n}{\mathrm{d}\lambda}\right|_{\lambda_0} = -0.18$), where dispersion of common materials is about 10 times larger than in the near infra-red ($\lambda_0 = 1054$ nm, BK7: $\lambda_0 \left.\frac{\mathrm{d}n}{\mathrm{d}\lambda}\right|_{\lambda_0} = -0.014$).
Due to the quadratic dependence of T_{PTD} on the beam size $r_{\max}$ and due to the large aperture needed in ultra-high peak power lasers, chromatic aberration significantly affects the performance of these systems and hence cannot be neglected for large beam diameters.

2.2 Pulse time delay in ultra-high peak power lasers

To date, pulse energy and peak power are mainly limited by laser-induced damage of the optical components. The weakest element in a high-power CPA laser system is usually the last grating of the pulse compressor. The fluence damage threshold φ_{τ_0} (fluence normal to the beam) of state-of-the-art multilayer dielectric (MLD) gratings is on the order of $\varphi_{\tau_0} \approx 0.6\ \mathrm{J/cm^2}$ at a pulse duration of $\tau_0 = 500$ fs. The subscript τ_0 indicates that the damage threshold varies with pulse duration. For MLD gratings φ_{τ_0} decreases monotonically with decreasing pulse duration. The maximum achievable pulse peak power at a pulse duration τ_0 for a top-hat intensity distribution is

$$P_{\max} = \frac{\pi \cdot r_{\max}^2 \cdot \varphi_{\tau_0}}{\tau_0}. \tag{8}$$

With Eq. (7) the ratio between the pulse time delay for a singlet lens and the duration of the undistorted pulse τ_0 is given by

$$\frac{T_{\mathrm{PTD}}}{\tau_0} = \frac{P_{\max}}{\varphi_{\tau_0}} \cdot \frac{-\lambda_0}{2\pi c f_0 (n_0 - 1)} \left.\frac{\mathrm{d}n}{\mathrm{d}\lambda}\right|_{\lambda_0}. \quad (9)$$

This ratio provides a good estimate when the pulse time delay and therefore chromatic aberration start to affect the achievable peak intensity in the focus significantly. As an example, for a fused-silica lens with a focal length of f_0 at the center wavelength of $\lambda_0 = 1.054\ \mu\mathrm{m}$ and $\lambda_0 \frac{\mathrm{d}n}{\mathrm{d}\lambda} = -0.014$, we obtain

$$\frac{T_{\mathrm{PTD}}}{\tau_0} \approx 2.5 \cdot 10^{-15} \frac{\mathrm{m}}{\mathrm{W}} \frac{P}{f_0}. \quad (10)$$

It should be noted that this includes only one lens for a beam radius of $r_{\max}$. Equation 10 shows that for petawatt class laser systems, $P \geq 10^{15} W$, the ratio T_{PTD}/τ_0 can easily exceed unity [9,18]. For the petawatt laser PHELIX [14], the beam is magnified with telescopes to a radius of $r_{\max} = 150\ \mathrm{mm}$ for the last amplification stage. The pulse is then guided with an additional transport telescope to the experimental area. Therefore, in PHELIX a total of five large aperture lenses are used. The sum of the pulse time delays from all lenses in the laser chain is $T_{\mathrm{PTD}} = 600$ fs. With the final pulse duration of $\tau_0 = 500$ fs, the ratio $T_{\mathrm{PTD}}/\tau_0 = 1.2$ indicates that the influence on the pulse spatio-temporal structure cannot be neglected.

3 Numerical wave optics propagation model

In the focal spot region, the spatial and temporal pulse form can not be described by geometrical optics. Hence, it is necessary to solve the diffraction integral. To calculate the propagation of ultra-short, broadband laser pulses with an arbitrary initial intensity distribution and arbitrary spatial phase aberrations, we have developed a numerical model based on the commercial wave optics propagation code GLAD. In the first step, we calculate the propagation of the initial field distribution $E(\omega_n, x_1, y_1, z_0)$ at z_0 to z for a set of monochromatic waves with frequencies ω_n with GLAD:

$$E(\omega_n, x_2, y_2, z) = \mathcal{P}\left[E(\omega_n, x_1, y_1, z_0)\right]. \quad (11)$$

Here $\mathcal{P}$ is a placeholder for the propagation calculation with GLAD. Spatial and chromatic aberrations and group velocity dispersion are included as frequency and space dependent phase shifts and can be separately switched on or off. The resulting complex fields are multiplied with the spectral amplitude $\psi(\Delta\omega)$ of the laser, with $\Delta\omega = \omega_n - \omega_0$ and ω_0 being the center frequency. To obtain the E-field in the time domain, the Fourier-transformation

$$E(t, x_2, y_2, z) = \mathrm{FFT}\{\psi(\Delta\omega) \cdot E(\omega, x_2, y_2, z)\}. \quad (12)$$

is performed. With our diffraction model, it is now possible to calculate the relative intensity change inside the focal region due to the pulse time delay. In the wave optics propagation code, we start with a flat pulse front perpendicular to the propagation direction and employ one Keplarian telescope to obtain a chromatic aberration equivalent to that of the actual laser chain. Finally, the pulse is focused with an ideal (i.e. achromatic) parabolic mirror. The following calculations are performed for typical PHELIX beam parameters if no other values are given: The spatial intensity profile is

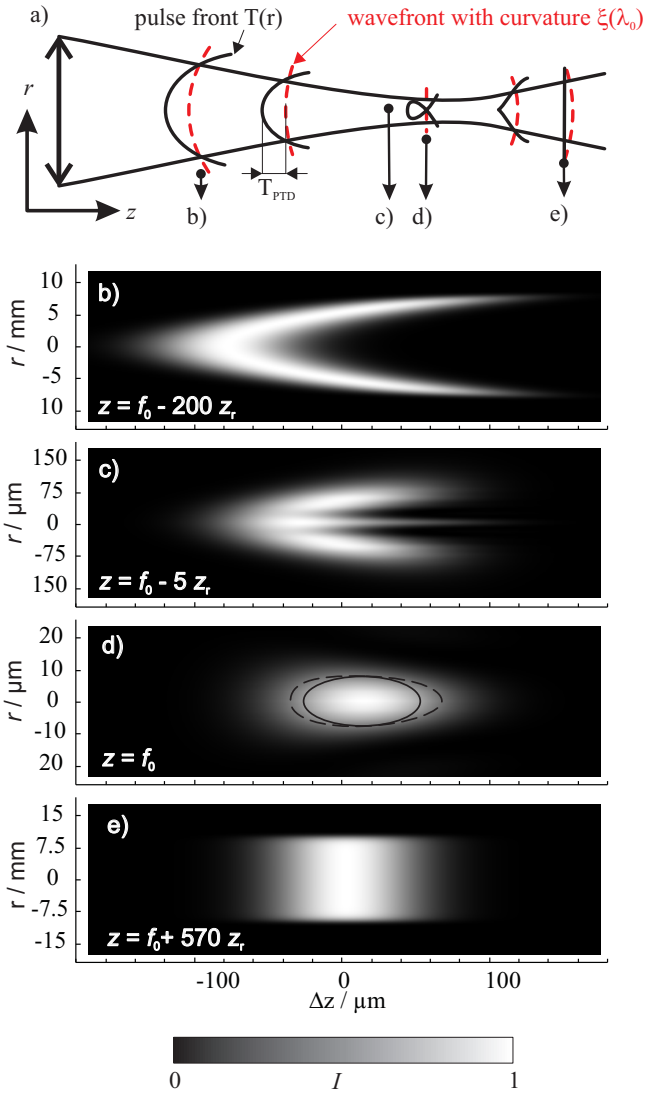

Fig. 3: Pulse front curvature resulting from a singlet lens with chromatic aberration in a $\tau_0 = 500$ fs beam, as predicted by **a** the geometrical optics model of Bor and **b-e** our wave optics short-pulse propagation model at four different z-positions after the lens. Parameters for the calculation are given in the text. z_r is the Raleigh length of the beam waist. **b** In the geometric-optical regime before reaching the focal region. **c** Five Rayleigh ranges before the focal region. **d** At focal position; the solid line indicates the half maximum contour of an undistorted pulse, the dashed line the half maximum contour of the distorted pulse. **e** At this z-position behind the focus, the group delay is $T(r) = 0$; the group delay caused by chromatic aberration $\left.\frac{\mathrm{d}\xi}{\mathrm{d}\lambda}\right|_{\lambda_0}$ compensates the curvature of the center wavelength, see Eq.4.

super-Gaussian of order $sg = 8$ according to:

$$I(r) = I_0 \cdot \exp\left[-\ln(2)\left(\frac{r}{r_{\max}}\right)^{2sg}\right], \qquad (13)$$

with a half-width half-maximum radius of $r_{\max} = 150$ mm and the center wavelength of $\lambda_0 = 1054$ nm. The spectral amplitude is assumed to have a Gaussian shape:

$$\psi(\Delta\omega) \propto \exp\left[-\frac{(\tau_0 \Delta\omega)^2}{8\ln(2)}\right], \qquad (14)$$

with the pulse duration $\tau_0 = 500$ fs (FWHM). The chromatic aberration for the entire system corresponds to a pulse time delay of $T_{\mathrm{PTD}} = 600$ fs. For the calculations an $f/\# = 3$ focusing was used. However, the results are independent of the f-number $f/\#$ of the final focusing mirror.

Figure 3 shows a comparison of results for the example of a singlet lens with chromatic aberration, as predicted by the geometrical optics model of Bor [8] in Fig. 3a and our wave optics short-pulse propagation model in Fig. 3b-e. The pictures show snapshots of the intensity pattern at various distances z after the lens. Far away from the focal region, the geometric optics treatment is accurate and the pulse front is the sum of the group delay caused by the phase curvature ξ_0 and the pulse time delay, Eq. (4), see Fig. 3b. The shortest pulse duration occurs at the z-position where $T(r) = 0$. Here the group delay caused by chromatic aberration $(\mathrm{d}\xi/\mathrm{d}\lambda)|_{\lambda_0}$ compensates with the group delay caused by the curvature of the center wavelength, i.e. $\xi_0 = \lambda_0 \left.\frac{\mathrm{d}\xi}{\mathrm{d}\lambda}\right|_{\lambda_0}$, see Fig. 3e. At these locations far from the focal region, geometrical optics and wave optics are in good agreement. Figure 3.c shows the pulse close to the geometrical focus. The pulse time delay is much larger than the delay due to the phase curvature and dominates the pulse form. Figure 3d shows the intensity distribution at the focus. In geometrical optics, the marginal rays have already passed the focus when the center rays reach it. This predicts a strongly distorted pattern. However, with the given pulse time delay of $T_{\mathrm{PTD}} = 600$ fs and the pulse duration of $\tau_0 = 500$ fs, wave optics predicts a nearly Gaussian profile in time with decreased intensity.

Figure 4 shows how the pulse time delay affects the peak intensity in the focal spot for pulse durations of $\tau_0 = 200$ fs, $\tau_0 = 500$ fs, and $\tau_0 = 900$ fs. As expected, the achievable focal intensity starts to get significantly reduced for $T_{\mathrm{PTD}} \gtrsim \tau_0$. For PHELIX, the intensity decrease is around 35%. The comparison of the curves shows that at equal ratios T_{PTD}/τ_0 the impact is slightly higher for longer pulses than for shorter ones.

Usually, a super-Gaussian spatial intensity distribution as described by Eq. (13) is used in a high-power laser chain. A super-Gaussian shape represents a reasonable compromise between the requirements for good energy extraction from the amplifiers and low propagation diffraction. The impact of chromatic aberration on the focused intensity depends on the spatial intensity distribution of the beam.

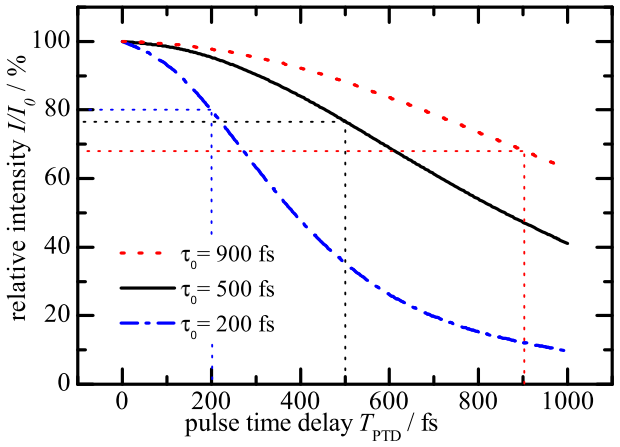

Fig. 4: Peak intensity I in the focal spot normalized to that in absence of chromatic aberration I_0, versus the pulse time delay T_{PTD} for initial pulse durations of $\tau_0 = 200$, 500, and 900 fs.

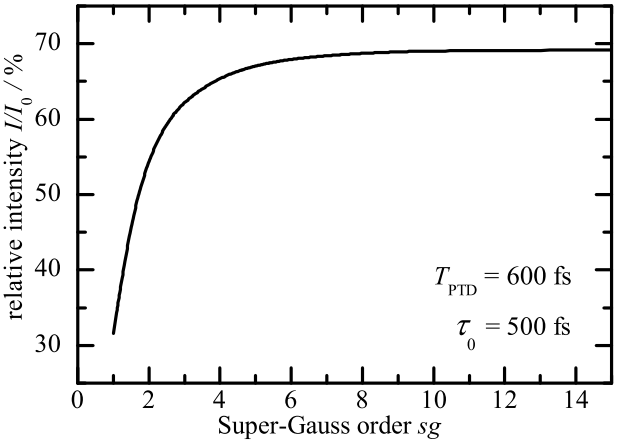

Fig. 5: Peak intensity I in the focal spot normalized to that in absence of chromatic aberration I_0, versus the super-Gaussian coefficient sg for $\tau_0 = 500$ fs pulse and the pulse time delay $T_{\mathrm{PTD}} = 600$ fs.

In Fig. 5 the influence of different super-Gaussian orders on the focused peak intensity is investigated for pulses with a duration of $\tau_0 = 500fs$ and a pulse time delay of $T_{PTD} = 600fs$. For the Gaussian beam with $sg = 1$, the intensity drops to 30 % compared to an aberration-free beam. For a beam of higher super-Gaussian order, the impact of the pulse time delay is weaker and the relative intensity converges to approximately 70 % for $sg \gtrsim 6$. The model shows that a super-Gaussian intensity distribution is more robust against chromatic aberration than a Gaussian intensity distribution.

Spatial aberrations also have an influence on the intensity achievable in the focus. In Fig. 6 the relative intensities for astigmatism, coma, and spherical aberration are shown. C is the Zernike coefficient in waves. The influence of the pulse time delay on the achievable intensity is lower in the presence of spatial aberrations. The calculation shows that the peak intensity of a pulse with chromatic and spatial aberra-

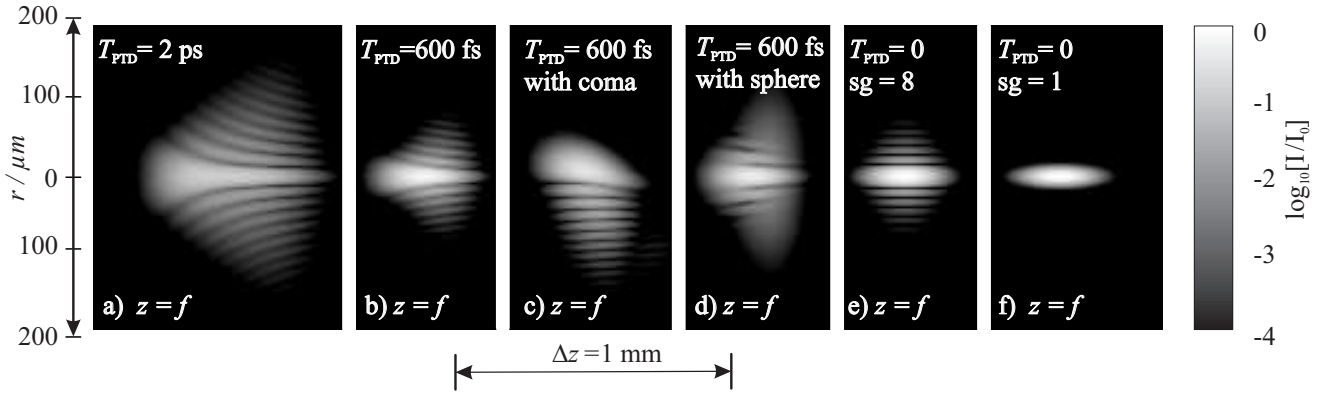

Fig. 7: Snapshots of the intensity distribution $\log_{10}[I/I_0]$ at the focal region. The initial pulse duration is $\tau_0 = 500$ fs with the super-Gaussian intensity shape, $sg = 8$. **a** $T_{\mathrm{PTD}} = 2$ ps, **b** $T_{\mathrm{PTD}} = 600$ fs, **c** $T_{\mathrm{PTD}} = 600$ fs with $C = 0.2\ \lambda$ coma aberration, **d** $T_{\mathrm{PTD}} = 600$ fs with $C = 0.2\ \lambda$ spherical aberration. **e** Without a pulse time delay, **f** focal spot of a Gaussian pulse in time and space without chromatic aberration.

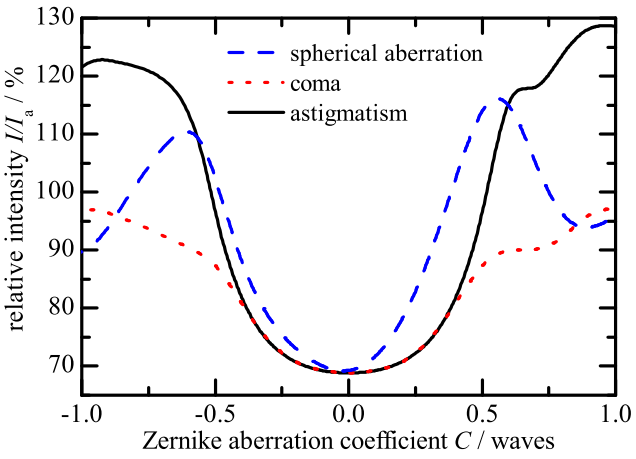

Fig. 6: Peak intensity I in the focal spot with chromatic and spatial aberrations ($T_{\mathrm{PTD}} = 600$ fs) normalized to the peak intensity I_a without chromatic aberration versus the spatial Zernike C coefficients for astigmatism, coma, and spherical aberration. Note, that I_a is the peak intensity in absence of chromatic aberration but in presence of spatial aberrations.

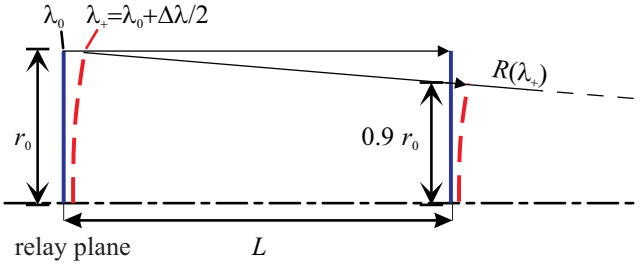

Fig. 8: Due to chromatic aberration, the beam diameter is a function of the wavelength after propagating the distance L. $R(\lambda_+) = 1/\xi(\lambda_+)$ is the radius of curvature of the wavefront at the wavelength λ_+.

tions can be higher than the intensity of a pulse with spatial aberration only, see also [12]. However, in this case the absolute achievable intensity is still much lower than in the case free of any aberration. In the presence of strong spatial phase aberrations, the chromatic aberration can be neglected and the correction of the spatial aberrations with adaptive optics has a larger benefit [16, 17]. The correction of chromatic aberration can significantly increase the focused intensity if the spatial beam quality is nearly diffraction limited.
For illustration, Fig. 7 shows some calculated examples of the spatio-temporal intensity distribution at the focal spot for various beam profiles, pulse time delays, and spatial aberrations.

4 Pre-compensation of pulse time delay

Chromatic aberration can be avoided by using achromats for all large-sized lenses. Even if such large achromats could be fabricated, this approach would be cost prohibitive. While compensation at large beam diameters seems a feasible option [18], a more cost-effective and easily implementable solution is the pre-compensation of the chromatic aberration of the telescope lenses at a position upstream in the beam path where the beam diameter is smaller. Pre-compensating the chromatic aberration imposes some restrictions on the subsequent laser chain. First, the laser beam in the amplifier sections will no longer be perfectly collimated and this could cause clipping at the rims of the laser disks and rods or reduce energy extraction because the beam does not fill the rods and disks completely. Second, the focal spot in the spatial filters will become larger and some wavelength may be clipped at the pinhole. We will discuss these two effects next.

4.1 Near field propagation

Optical elements like amplifier rods are placed in between the magnifying telescopes which relay-image the laser beam. The length L where an optical element should be placed around the relay-imaged plane is limited by the requirement on the Fresnel number:

$$F = \frac{r^2}{\lambda L} \gg 1. \tag{15}$$

As a simple criterion limiting the propagation length in the presence of chromatic aberration we require the beam radius not to change significantly (e.g. not more than 10%) for all wavelengths within the spectrum of the short pulse (e.g. the FWHM spectral bandwidth $\Delta\lambda$), see Fig. 8:

$$L \leq 0.1R\,(\lambda) \quad \text{for } \lambda_0 - \frac{\Delta\lambda}{2} \leq \lambda \leq \lambda_0 + \frac{\Delta\lambda}{2}. \tag{16}$$

With the time-bandwidth product $\tau_0\Delta\omega = 4\ln(2)$ and Eq. (5) (with $\xi_0 = 0$, i.e. a collimated beam), we obtain

$$\frac{0.1 \cdot 2\pi}{4\ln(2)} \frac{\tau_0}{T_{\mathrm{PTD}}} \cdot F \geq 1. \tag{17}$$

This new criterion for the allowed free-propagation distances requires to carefully review the optical layout of the laser chain. In the PHELIX laser, $F \gtrsim 100$ holds true for beam radii of $\geq 1\ \mathrm{cm}$. This allows pre-compensation of pulse time delays of several τ_0.

4.2 Limits to spatial filtering

Spatial filtering along a high-power laser chain is of crucial importance in order to ensure that high spatial frequency modulations of the beam profile are filtered before they undergo further amplification and non-linear self-focusing. Chromatic aberration results in a longitudinal shift of the focal position for the different wavelengths of the amplified pulse. To prevent spectral filtering by the pinhole (which we assume to be positioned at the waist of the center wavelength), th the pinhole diameter d_{p} has to be enlarged as compared to the aberration free case. To ensure that the transmission exceeds 99% over the pulse spectrum $\Delta\lambda$, we require for the pinhole diameter $d\mathrm{p}$ of a Gaussian beam [19]

$$d_{\mathrm{p}} \geq 3w, \tag{18}$$

where the $1/\mathrm{e}^2$-intensity beam radius is given by

$$w(z) = w_0\sqrt{1 + \left(\frac{\Delta z \lambda_0}{\pi w_0^2}\right)^2}. \tag{19}$$

With the waist size $w_0 = \frac{\lambda_0}{\pi}\frac{f}{w_{\mathrm{lens}}}$ and the distance from the waist Δz as in Eq.(2), it follows that

$$d_{\mathrm{p}} \geq 3w_0\sqrt{1 + \left(2\ln(2)\frac{T_{\mathrm{PTD}}}{\tau_0}\right)^2}. \tag{20}$$

Comparing Eq. (20) and Eq. (18) shows that with a non-zero pulse time delay the pinhole diameter has to be increased in order to prevent spectral narrowing. This requirement is usually met in high-power lasers because the pinhole diameters are chosen at least five times larger than the diffraction limit in order to allow for shot-to-shot fluctuation of the beam pointing.

4.3 Pre-compensation set-up

One obvious solution to pre-compensate chromatic aberration of large aperture positive lenses is the use of a negative lens in combination with a spherical mirror. In the compensation set-up proposed in Fig. 9a, a double pass through two negative lenses is realized by quarter-wave plates and a polarizing beam-splitter. Besides doubling the amount of chromatic aberration, the set-up has the advantage that it can simply be inserted into the laser chain without changing beam size or direction. However, due to the rather small chromatic aberration of common optical glasses the achievable pulse time delay is limited by the available f-number. Low f-numbers are required to compensate chromatic aberration at small beam diameters. Spatial aberrations of such a low $f/\#$ lens, namely spherical aberration, can be quite severe and must also be taken into account.

A better approach to create large amounts of chromatic aberration is to use a diffractive lens instead of a refractive lens. A diffractive Fresnel zone lens is realized with a circular amplitude or phase modulation. The radius of the $N\mathrm{th}$ zone ring is given by $\rho_N = \sqrt{f_0 \cdot \lambda \cdot N}$. For a given Fresnel zone lens with the focal length $f_0 = \rho_N^2/(N\lambda)$ the chromatic aberration is:

$$\frac{\mathrm{d}f}{\mathrm{d}\lambda} = \frac{-f_0}{\lambda}. \tag{21}$$

With Eq. (6) and Eq. (21) the pulse time delay for a Fresnel zone lens follows

$$T_{\mathrm{PTD,Fresnel}} = -\frac{r_{\mathrm{max}}^2}{2cf_0}. \tag{22}$$

As can be seen from Eqs. (7, 22), the pulse time delay produced by both refractive and diffractive lenses scales inversely proportional to the lens $f/\#$. For a given $f/\#$ and radius, the value of the pulse time delay created by a diffractive lens is

$$\left(\frac{\lambda_0}{(n-1)}\frac{\mathrm{d}n}{\mathrm{d}\lambda}\right)^{-1} \approx 30 \tag{23}$$

times larger than that of a refractive lens. Thus using a diffractive lens instead of a refractive lens, correction of a certain amount of pulse time delay at a small beam diameter can be realized with significantly larger $f/\#$s. Also, remaining spatial aberrations can easily be corrected by the zone lens itself. Calculations done with the program GSOLVER show that a blazed structure with eight discrete values has an efficiency better than 90%. The influence of the polarization on the diffraction efficiency can be neglected if the bandwidth is not larger than a few nm. A Galilean telescope with $\mathrm{f}/\# = 25$ lenses and approximately unity magnification can correct a pulse time delay of $600\ \mathrm{fs}$ for a beam of $2\ \mathrm{cm}$ radius. Figure 9b shows a possible correction set-up that combines a negative refractive lens with a positive Fresnel zone lens. By etching the Fresnel zone lens directly on the flat side of a plano-concave lens, a single correction element can be realized.

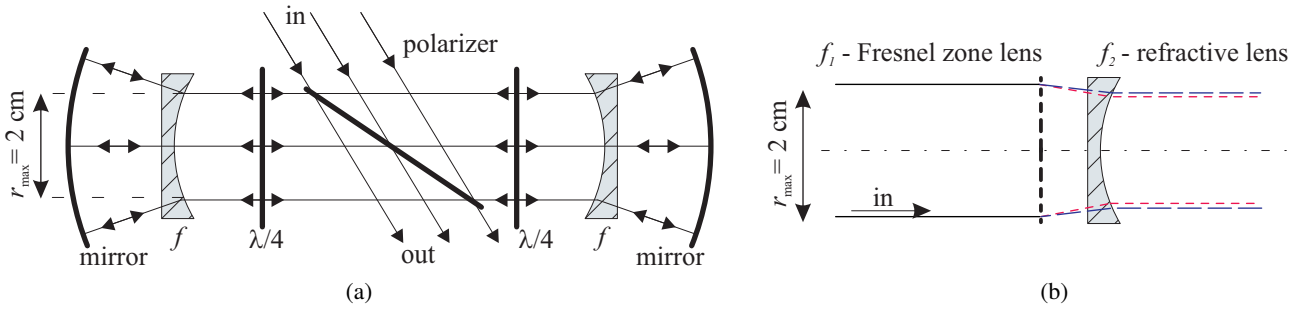

Fig. 9: Possible compensation set-ups. **a** Two negative lenses introduce a negative pulse time delay; each lens is passed two times. **b** Fresnel zone lens with a negative refractive lens in a Galileian telescope. If the focal length is chosen to be $-f_2 \approx f_1$, the beam diameter is not changed significantly. Due to the large negative dispersion of a Fresnel zone lens, a compensation with larger $f/\#$ lenses is possible compared to **a** at the same beam diameter.

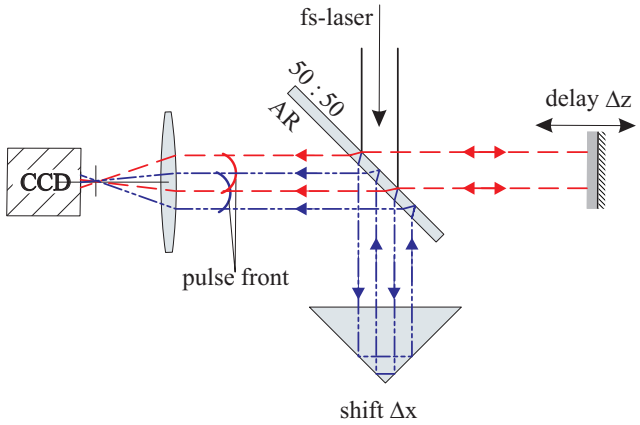

Fig. 10: In the shifted-field autocorrelator, one arm is shifted so that one half of the beam interferes with the other half. Interference occurs only where the pulses overlap.

5 Measurement set-up for pulse time delay

In order to validate the performance of a correction set-up for chromatic aberration, an accurate measurement of the remaining pulse time delay of the laser system is required. A measurement of the total pulse duration in the far-field is not appropriate as the pulse lengthening due to pulse time delay can not be distinguished from other effects. However, a curved pulse front can be detected by overlapping the pulse with an undistorted reference pulse. The pulse front distortion is revealed by an interference pattern which is spatially confined as a consequence of the limited longitudinal extent of the short pulse. Alternatively, the spatially varying delay between the pulse to be characterized and the reference pulse can be measured by space-resolved spectral interference or space-resolved intensity autocorrelation [20–22].

Working with a reference pulse is no longer feasible if the pulse time delay of a laser chain around 100 m long has to be determined. Therefore, we developed a measurement device that is self-referencing and can hence be used at any position within the laser chain. This device is a modification of the "inverted field autocorrelator" setup reported by Pretzler *et al.* [23]. In the Michelson interferometer shown in Fig. 10, the beam in one of the interferometer arms is laterally shifted by the distance Δx. This way, one half of the beam interferes with the other half ("shifted-field autocorrelation"). While an undistorted pulse yields an interference contrast which is constant over the whole overlapping region, a beam with a curved pulse front will show interference fringes only in the region given by the intersection of the two pulses. This is also true for a chirped pulse. By varying the optical path length in one of the interferometer arms, the form of the pulse front can be inferred. However, as the pulse is used as its own reference, symmetry about the axis perpendicular to the lateral shift has to be assumed. This is usually the case. For first-order chromatic aberration, the intersection of two paraboloidal pulse fronts described by

$$z_1(x,y) = -a \cdot (x^2 + y^2) + \Delta z, \tag{24}$$
$$z_2(x,y) = -a \cdot ((x - \Delta x)^2 + y^2), \tag{25}$$

is a line perpendicular to the direction of the lateral shift. Varying the delay Δz, the line shifts according to

$$x = \frac{\Delta x}{2} + \frac{\Delta z}{2a\Delta x}. \tag{26}$$

The pulse front curvature a can be derived from the slope $m = \mathrm{d}x/\mathrm{d}\Delta z = 1/(2a\Delta x)$ of Eq. (26). Finally, the pulse time delay

$$T_{\mathrm{PTD}} = \frac{a \cdot r_{\mathrm{max}}^2}{c} \tag{27}$$

can be determined.

Figure 11 shows two sample interferograms from a test of the shifted-field autocorrelator. In this measurement, a pulse of an initial duration of $\tau_0 = 100$ fs from a Coherent MIRA fs-laser was used. The pulse time delay of 1.2 ps was introduced by a magnifying telescope which expands the beam diameter from 10 mm to 300 mm. Then the beam is reflected back through the telescope and the pulse time delay is measured with the shifted-field autocorrelator at a beam diameter of 10 mm, see Fig. 12. The shift of the maximum interference contrast as a function of the temporal delay is plotted in Fig. 13. The theoretical line fits very well to the measured positions of maximum contrast.

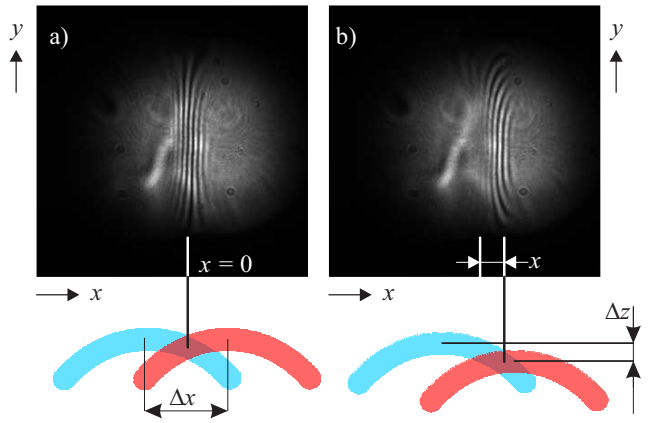

Fig. 11: Interference for two different delays. Fringes are only visible within the region of spatial and temporal overlap of the two pulses. **a** The pulses are not delayed, **b** one pulse is delayed with respect to the other by $\Delta z/c$.

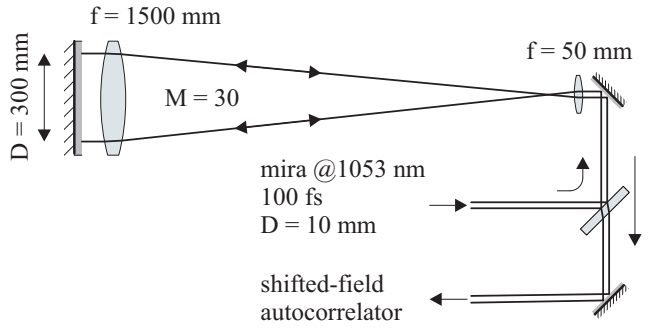

Fig. 12: Setup to introduce the pulse time delay of 1.2 ps on the fs-laser pulse. The beam passes the large lens of diameter $D = 300$ mm in the spatial magnifying telescope twice.

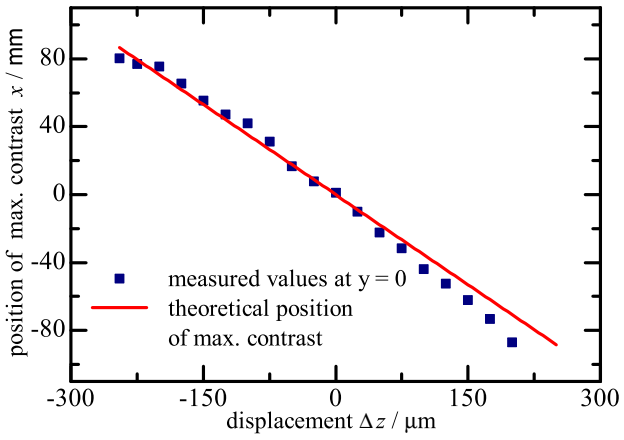

Fig. 13: Measured intersection of two pulses in the shifted-field autocorrelator. Pulse time delay for the measured set-up is 1.2 ps, pulse duration of the probe laser is 100 fs.

6 Summary

We have demonstrated that in petawatt lasers chromatic aberration is a non-negligible effect that significantly reduces the focal intensity. In consideration of the limitations discussed in section 4, a correction of chromatic aberration of an entire laser chain can be achieved by pre-compensation before the laser beam is expanded to fit the large amplifiers. We propose two compensation schemes. While the first uses standard components in a complex set-up, the second uses a diffractive element in a simpler setup. We have introduced and demonstrated a new method to measure the curved pulse front with a shifted-field autocorrelator. This set-up is self referencing and allows the measurement of the pulse time delay of chirped and unchirped beams.

References

1. K.W.D. Ledingham, P. McKenna, R.P. Singhal, Science **5622,** 1107 (2003)
2. S.P.D. Mangles, C.D. Murphy, Z. Najmudin, A.G.R. Thomas, J.L. Collier, A.E. Dangor, E.J. Divall, P.S. Foster, J.G. Gallacher, J.G. Hooker, D.A. Jaroszynski, A.J. Langley, W.B Mori, P.A. Norreys, F.S. Tsung, R. Viskup, B.R. Walton, K. Krushelnick, Nature **431,** 535 (2004)
3. C.G.R. Geddes, C. Toth, J. van Tilborg, E. Esarey, C.B. Schroeder, D. Bruhwiler, C. Nieter, J. Cary, W.P. Leemans, Nature **431,** 538 (2004)
4. J. Faure, Y. Glinec, A. Pukhov, S. Kiselev, S. Gordienko, E. Lefebvre, J.P. Rousseau, F. Burgy, V. Malka, Nature **431,** 541 (2004)
5. M.D. Perry, D. Pennington, B.C. Stuart, G. Tietbohl, J.A. Britten, C. Brown, S. Herman, B. Golick, M. Kartz, J. Miller, H.P. Powell, M. Vergino, V. Yanovsky, Opt. Lett. **24,** 160 (1999)
6. D. Strickland, G. Mourou, Opt. Commun. **56,** 219 (1985)
7. J.D. Zuegel, S. Borneis, C. Barty, B. LeGarrec, C. Danson, N. Miyanaga, P.K. Rambo, C. LeBlanc, T.J. Kessler, A.W. Schmid, L.J. Waxer, J.H. Kelly, B. Kruschwitz, R. Jungquist, E. Moses, J. Britten, I. Jovanovic, J. Dawson, N. Blanchot, Fusion Sci. Technol. **49**, 453 (2005)
8. Z. Bor: J. Mod. Opt. **35,** 1907 (1988)
9. N. Blanchot, E. Bignon, H. CoÃŕÂ£ÅŞ, E. Freysz, E. Hugonnot, S. Hulin, G. Marre, G. Mennerat, A. Migus, S. Montant, J. NÃŕÂ£ÅŞuport, S. Noailles, C. Rouyer, C. RulliÃŕÂ£ÅŞe, C. Sauteret, E. SibÃŕÂ£ÅŞ L. Videau, P. Vivini, Technical issues in the MPWHE-LIL laser project, in *Proc. of International Conference on Ultrahigh Intensity Lasers (ICUIL) 2004*, 3
10. T.A. Planchon, S. Ferré, G. Hamoniaux, G. Chériaux, J.P. Chambaret *Opt. Lett.* **29,** 2300 (2004)
11. M. Kempe, U. Stamm, B. Wilhelmi, W. Rudolph, J. Opt. Soc. Am. B **9,** 1158 (1992)
12. M. Kempe, W. Rudoph, Opt. Lett. **18,** 137 (1993)
13. U. Fuchs, U.D. Zeitner, A. Tünnermann, Opt. Expr. **10** 3852 (2005)
14. P. Neumayer, R. Bock, S. Borneis, E. Brambrink, H. Brand, J. Caird, E.M. Campbell, E. Gaul, S. Goette, C. HÃŕÂ£ÅŞner, T. Hahn, H.-M. Heuck, D.H.H. Hoffmann, D. Javorkova, H. Kluge, T. Khl, S. Kunzer, T. Merz, E. Onkels, M.D. Perry, D. Reemts, M. Roth, S. Samek, F. Schrader, W. Seelig, A. Tauschwitz, R. Thiel, D. Ursescu, P. Wiewior, U. Wittrock, B. Zielbauer, Laser Part. Beams **23,** 385 (2005)

15. Applied Optics Research *GLAD Theorie Manual*,[www.aor.com]
16. H.-M. Heuck, E.W. Gaul, C. Häfner, T. Kühl, P. Wiewior, U. Wittrock, *Adaptive Optics for Industry and Medicine* (Springer Proc. Phys. **102**)(Springer, Berlin, 2005) p.283-290
17. U. Wittrock, I. Buske, H.-M. Heuck, *Laser Resonator and Beam Control VI* (Springer Proc. SPIE **4969**)(Springer, Berlin, 2003) 122-136
18. E.W. Gaul, T. Ditmire, M.D. Martinez, S. Douglas, D. Gorski, W. Henderson, G.R. Hays, A. Erlandson, J.A. Caird, I. Jovanovic, C. Ebbers, W. Molander, Design of the Texas petawatt laser, in *Proc. Conf. Lasers and Electro-Optics (CLEO) 2005*, JFB2
19. A.E. Siegmann, *Lasers* (University Science Books, Sausalito, CA, 1986) 666
20. R. Netz, T. Feurer, R. Wolleschensky, R. Sauerbrey: Appl. Phys. B. **70,** 833 (2000)
21. Z. Bor, Z. Gogolak, G. Szabo: Opt. Lett. **14,** 862 (1989)
22. S. Szatmari, G. Khnle: Opt. Commun. **69,** 60 (1988)
23. G. Pretzler, A. Kasper, K.J. Witte: Appl. Phys. B. **70,** 1 (2000)